REPORT DOCUMENTATION PAGE

Form Approved
OMB No. 0704-0188

PLEASE DO NOT RETURN YOUR FORM TO THE ABOVE ORGANIZATION.

1. REPORT DATE *(DD-MM-YYYY)*	2. REPORT TYPE	3. DATES COVERED *(From - To)*
28-06-2006	Journal Article (refeered)	

4. TITLE AND SUBTITLE

Doppler Frequency Shift in Ocean Wave Measurement: Frequency Downshift of a Spectral Feature Due to Convection by Surface Wave Orbital Velocity

5a. CONTRACT NUMBER

5b. GRANT NUMBER

5c. PROGRAM ELEMENT NUMBER

PE062435N

6. AUTHOR(S)

Paul Hwang

5d. PROJECT NUMBER

5e. TASK NUMBER

5f. WORK UNIT NUMBER

73-6628-85-5

7. PERFORMING ORGANIZATION NAME(S) AND ADDRESS(ES)

Naval Research Laboratory
Oceanography Division
Stennis Space Center, MS 39529-5004

8. PERFORMING ORGANIZATION REPORT NUMBER

NRL/JA/7330-05-5252

9. SPONSORING/MONITORING AGENCY NAME(S) AND ADDRESS(ES)

Office of Naval Research
800 N. Quincy St.
Arlington, VA 22217-5660

10. SPONSOR/MONITOR'S ACRONYM(S)

ONR

11. SPONSOR/MONITOR'S REPORT NUMBER(S)

12. DISTRIBUTION/AVAILABILITY STATEMENT

Approved for public release, distribution is unlimited.

13. SUPPLEMENTARY NOTES

14. ABSTRACT

Because the Jacobian connecting wave number to frequency conversion is nonlinear, in the presence of background waves even without a mean current a wave number spectral component does not appear at he expected intrinsic frequency in the frequency spectrum measured by a stationary probe. The advection of the wave number component by the orbital current of background waves produces a net downshift in the encounter frequency. Comparison with laboratory measurements shows that the effect is important in low-wind conditions. As wind speed increases, the frequency downshift due to orbital advection becomes less recognizable.

15. SUBJECT TERMS

wave spectrum, doppler frequency shift, orbital velocity, frequency-to-wavenumber conversion

16. SECURITY CLASSIFICATION OF:			17. LIMITATION OF ABSTRACT	18. NUMBER OF PAGES	19a. NAME OF RESPONSIBLE PERSON
a. REPORT	b. ABSTRACT	c. THIS PAGE			Paul Hwang
Unclassified	Unclassified	Unclassified	UL	4	19b. TELEPHONE NUMBER *(Include area code)* (202) 404-0800

JOURNAL OF GEOPHYSICAL RESEARCH, VOL. 111, C06033, doi:10.1029/2005JC003072, 2006

Doppler frequency shift in ocean wave measurements: Frequency downshift of a fixed spectral wave number component by advection of wave orbital velocity

Paul A. Hwang[1,2]

Received 25 May 2005; revised 15 February 2006; accepted 21 March 2006; published 24 June 2006.

[1] Because the Jacobian connecting wave number to frequency conversion is nonlinear, in the presence of background waves even without a mean current a wave number spectral component does not appear at the expected intrinsic frequency in the frequency spectrum measured by a stationary probe. The advection of the wave number component by the orbital current of background waves produces a net downshift in the encounter frequency. Comparison with laboratory measurements shows that the effect is important in low-wind conditions. As wind speed increases, the frequency downshift due to orbital advection becomes less recognizable.

Citation: Hwang, P. A. (2006), Doppler frequency shift in ocean wave measurements: Frequency downshift of a fixed spectral wave number component by advection of wave orbital velocity, *J. Geophys. Res.*, *111*, C06033, doi:10.1029/2005JC003072.

1. Introduction

[2] The ocean surface roughness is contributed mainly by surface waves of intermediate and short length scales. A recent study of the wave number spectrum of ocean surface waves shows that more than 77 percent of the mean square slope of surface gravity waves is contributed by waves 0.02 to 6 m long [*Hwang*, 2005]. These wavelengths are of great interest to ocean remote sensing by microwave radars because Bragg resonance is the primary mechanism scattering the impinging radar waves back to the receiving antenna for moderate incident angles frequently used in radar remote sensing [e.g., *Wright*, 1966, 1968]. The Bragg wavelength is on the same order of the radar wavelength.

[3] To compute the surface roughness from a wave spectrum, the correct wave number associated with a spectral component needs to be determined. Because most surface wave measurements are conducted using stationary sensors, a difficult issue for quantifying the mean square slope of intermediate and short-scale waves is the Doppler frequency shift for determining the length scale of a measured encounter frequency spectral component. In this paper, an analysis is presented on the wave number and frequency spectra computed from simultaneous measurements of the space-time series of surface wave slopes. The wave number spectrum represents the surface roughness property sensed by radar, and the frequency spectrum represents the counterpart measured by a conventional stationary wave sensor. Significant difference in the spectral properties can be detected. In particular, identifiable features in the wave number spectrum show an obvious frequency downshift in the frequency spectrum (section 2). An interpretation of this result is offered. Briefly, when the orbital velocity of background waves is considered in the Jacobian connecting the wave number to frequency conversion, a net frequency downshift is realized after averaging over integral cycles of long waves (section 3). The magnitude of the computed frequency downshift is in reasonable agreement with laboratory observations in low-wind conditions. As wind speed increases, the frequency downshift due to orbital advection becomes difficult to recognize. A summary is presented in section 4.

2. Observations of Frequency Downshift of Spectral Features

[4] Wind-generated waves riding on mechanically generated background waves were measured in a wind-wave facility. A scanning slope sensor records the space-time evolution of small-scale waves. The design and operating principles of the sensor system have been presented in an earlier publication [*Hwang et al.*, 1993] so only a brief description of the experiment is given here. The data are acquired in the Air-Sea Interaction Laboratory, University of Delaware. The wind fetch of the measurement station is 16 m, which is near the midsection of the 1-m-wide wind-wave flume. The water depth and the air duct clearance are both 0.75 m. The scanning laser slope sensor measures the downwind and crosswind components of the wave slope along a 0.12-m linear segment aligned in the wind direction at the center of the flume. The linear segment is sampled at 0.002 m intervals, and the linear scanning pattern is repeated at a rate of 200 scans per second. The wave height of the background mechanical waves is 0.045 m, and the wave period 1 s. Wind waves are generated for eight wind speeds (wind friction velocities): 0 (0), 1.98 (0.11), 3.47 (0.18), 5.11 (0.26), 6.78 (0.33), 8.37 (0.43), 9.95 (0.55), and

[1]Oceanography Division, Naval Research Laboratory, Stennis Space Center, Mississippi, USA.
[2]Now at Remote Sensing Division, Naval Research Laboratory, Washington, D.C., USA.

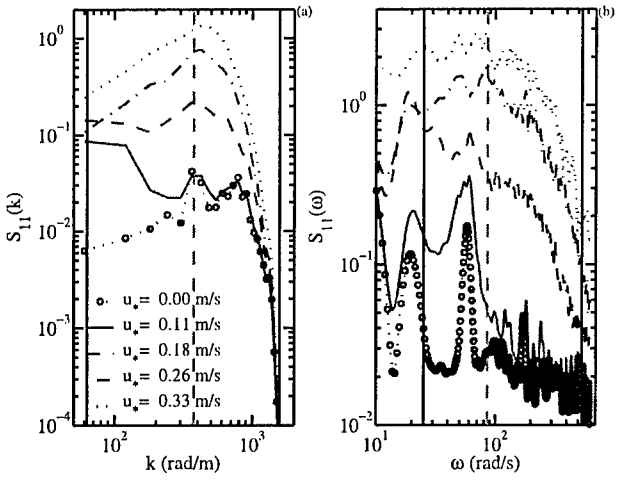

Figure 1. The curvature spectra of short waves computed from simultaneous spatiotemporal measurements of surface slopes obtained by a scanning laser slope sensor in (a) wave number domain and (b) frequency domain.

11.62 (0.68) m/s. Figure 1 of *Hwang* [2002] shows the spatiotemporal images of the measured surface slopes for the eight wind conditions.

[5] Figure 1a shows the wave number spectra of the surface curvature, $S_{11}(k)$, obtained by processing the spatial series of the spatiotemporal slope data, and Figure 1b shows the frequency spectra processed from the temporal series of the same data. In the wave number spectra a distinctive spectral feature can be detected near the wave number of minimal phase speed, k_{cm} (374 rad/m), marked by a vertical dashed line in Figure 1a. The spectral feature shows up as a local bump in the spectrum at the two lowest wind conditions. As wind speed increases, the wave number range of the bump broadens. Surprisingly, such spectral bumps are conspicuously missing in the frequency spectra at the corresponding intrinsic frequency (ω_{0cm} = 85 rad/s, marked by a vertical dashed line in Figure 1b). Note that the high sample rate (200 Hz) and long data record (10 s) in the temporal measurement resolve a much wider range of the wave frequency components than that of the spatial measurement. To aid the comparison two solid lines at 0.004 and 0.1 m wavelength components, close to the full range of the wave number resolution of the scanning laser slope sensor, are superimposed in Figure 1. Searching for similar spectral bumps in the frequency spectra near ω_{0cm}, it is suggestive that the closest frequency spectral features are those near 60 rad/s. These prominent features in the frequency spectra are not found at the expected wave number (k = 252 rad/m) in the wave number spectra. The apparent frequency downshift of the spectral features described above is not due to a mean drift current, induced either by wave nonlinearity or surface wind drift, which would have shifted the spectral feature toward higher frequencies. A possible explanation is offered in the following.

3. Frequency Downshift Due to Orbital Advection

[6] In the presence of an ambient current the dispersion relation connecting the wave number, $\boldsymbol{k}$, and the encounter frequency, ω, of a wave component measured by a stationary probe is

$$\omega = \left(gk + \tau k^3\right)^{0.5} + \boldsymbol{u} \bullet \boldsymbol{k}, \tag{1}$$

where the first term on the right hand side is the intrinsic frequency, $\omega_0 = (gk + \tau k^3)^{0.5}$, and the second term is the current-induced Doppler frequency shift, $\Delta\omega = \boldsymbol{u} \bullet \boldsymbol{k}$ ($\boldsymbol{u}$ is the surface current vector with modulus u), g is the gravitational acceleration, τ is the ratio between surface tension and water density, and k is the modulus of the wave number vector $\boldsymbol{k}$.

[7] The connection between frequency and wave number spectra can be written as

$$S(\omega)d\omega = S(k)dk. \tag{2}$$

Considering the simple case of one-dimensional flow with the wave-induced orbital velocity represented by a sinusoidal function with amplitude u_0 and phase ϕ and assuming that the period of the orbital velocity is much longer than the period of the advected wave component so that the orbital current can be treated as piecewise constant, then the dispersion relation (equation (1)) becomes

$$\omega = \left(gk + \tau k^3\right)^{0.5} + u_0 k\cos\phi + u_s k, \tag{3}$$

where u_s is the mean drift current, and the Jacobian in (2) is

$$J = \left|\frac{dk}{d\omega}\right| = \left|\frac{1}{c_g + u}\right| = \left|\frac{1}{c_g + u_0\cos\phi + u_s}\right|. \tag{4}$$

[8] It is clear from inspecting (4) that J is not a linear function of ϕ, and therefore the effect of orbital velocity on wave number to frequency conversion does not vanish after averaging over integral cycles of the orbital motion. Figures 2a–2b depict the "trajectory" in the frequency domain of a single wave number component subjected to advection by the orbital motion of a monochromatic background wave train. The amplitude of the orbital velocity, u_0 = 0.15 m/s, is relatively mild, but the impact on the frequency spectral representation is quite severe. Instead of a one-to-one transformation from wave number to frequency, the orbital motion smears the signature of the wave number component over a range of frequencies with a bandwidth proportional to $u_0 k$. The Jacobian amplifies the spectral level when the encounter frequency is less than the intrinsic frequency (counter current) and attenuates the spectral level for the other half-cycle when the current is in the same propagation direction of the advected wave component. For reference, the trajectory of the wave number component within 15 degree of the long-wave crest (trough) phase is marked with up-pointing (down-pointing) triangles in Figure 2. The variation in the magnitude of the Jacobian and the encounter frequency at different phases of the long waves is usually of $O(1)$ or larger for intermediate and short-scale waves. The frequency spectrum of a single wave number component averaged over one full cycle of the long-wave orbital motion shows a net frequency downshift from the expected intrinsic frequency as a result of the

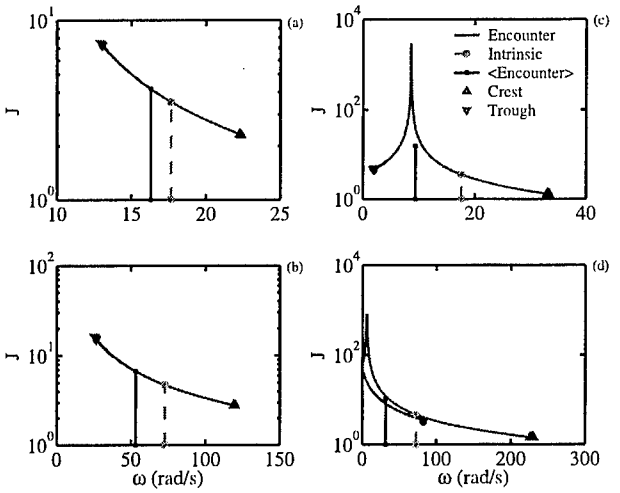

Figure 2. Examples of the trajectory in the frequency space of a wave number spectral component advected by a sinusoidal orbital current, presented in terms of the Jacobian of the wave number to frequency conversion. The nonlinearity of J causes a net frequency downshift in the average spectrum. (a) $u_0 = 0.15$ m/s, $k = 31.6$ rad/m, (b) $u_0 = 0.15$ m/s, $k = 316$ rad/m, (c) $u_0 = 0.5$ m/s, $k = 31.6$ rad/m, and (d) $u_0 = 0.5$ m/s, $k = 316$ rad/m. Up-pointing (down-pointing) triangles are placed on the trajectory curves to indicate the long-wave phases within ±15° of the long-wave crest (trough).

nonlinearity of the Jacobian. This can be quantified by comparing the weighted average frequency and Jacobian for a fixed wave number, defined as

$$\langle\omega\rangle_k = \left[\int \omega J(\omega)d\omega \Big/ \int J(\omega)d\omega\right]_k, \tag{5}$$

$$\langle J\rangle_k = \left[\int \omega J(\omega)d\omega\right]_k \Big/ \langle\omega\rangle_k, \tag{6}$$

with the corresponding intrinsic frequency and Jacobian in the absence of currents. For the examples shown in Figure 2, $\langle\omega\rangle_k$ (marked by vertical solid line segments) and ω_0 (marked by vertical dashed line segments in Figure 2 and in parentheses in the following numbers) are 16.3 (17.7) rad/s for $k = 31.6$ rad/m and 53.1 (72.9) for $k = 316$ rad/m.

[9] When the orbital velocity generated by the background wave field is large compared to the group velocity of the advected wave component, the encounter frequency can become zero or even negative. The Jacobian becomes singular at the phase angles where $c_g + u_0\cos\phi + u_s = 0$. Figures 2c–2d show the results repeating the computation for the same wave number components shown in Figures 2a–2b but with $u_0 = 0.5$ m/s. Because a stationary sensor cannot distinguish between negative and positive frequencies, when the encounter frequency computed from the dispersion relation (equation (2)) becomes negative, the spectral contribution is projected at the absolute value of the encounter frequency. A few noticeable differences between Figures 2c–2d and 2a–2b are the expanded frequency range of the orbital advection by the stronger velocity and the dramatic increase in the magnitude of the Jacobian near the singularity that distorts the resulting average frequency spectrum. For this case, the weighted average frequency and the intrinsic frequency (in parentheses) are 9.5 (17.7) rad/s for $k = 31.6$ rad/m and 14.2 (72.9) rad/s for $k = 316$ rad/m.

[10] Figure 3a shows the weighted average frequency for a range of wave numbers (from 1 to 1000 rad/m) and three different current amplitudes (0, 0.15, and 0.17 m/s) of the orbital velocity. The corresponding average Jacobian is shown in Figure 3b. As expected, the spectral distortion due to Doppler frequency shift by orbital velocities is most serious in the neighborhood of minimum group velocity ($c_{gm} = 0.18$ m/s, $k_{cgm} = 145$ rad/m, $\omega_{0cgm} = 41$ rad/s).

[11] The dimensionless wave number spectra, $B(k)$, obtained from spatial measurement in four different wind speeds are compared with those converted from the frequency spectra (Figure 4). The conversion is carried out with and without considering the advection of orbital velocity, shown by curves designated with $u_0 = 0.17$ m/s and 0 m/s, respectively. At lower wind speeds the placement of the spectral feature (local bump) is more accurately produced by the procedure that considers the orbital velocity in the Jacobian and the encounter frequency (Figures 4a–4b). As wind speed increases, the spectral features are more difficult to identify. The converted spectra including the effect of orbital convection in fact deviate more from the reference spectra obtained from spatial measurements (Figure 4c–4d), possibly because the simplification of the background wave field.

[12] Numerical computations that include the effects of short-wave modulation by background waves [e.g., *Longuet-Higgins*, 1960; *Phillips*, 1977, 1981, 1984] and the directional distribution of short waves were also carried out. These effects introduce secondary modification to the magnitude of the Doppler frequency shift and the Jacobian.

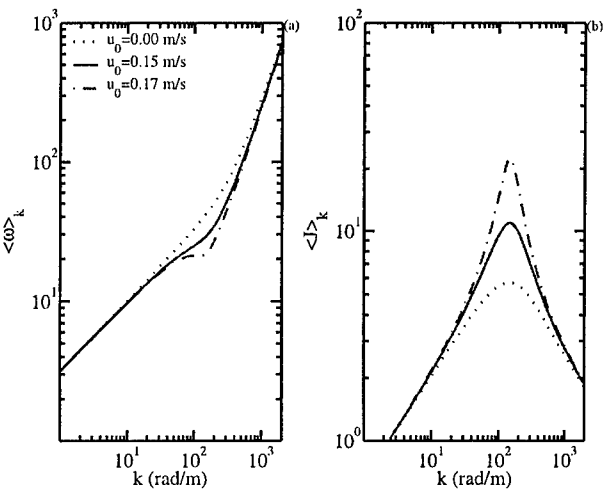

Figure 3. The net effect of Doppler frequency shift caused by orbital velocities on (a) the average frequency and (b) the Jacobian.

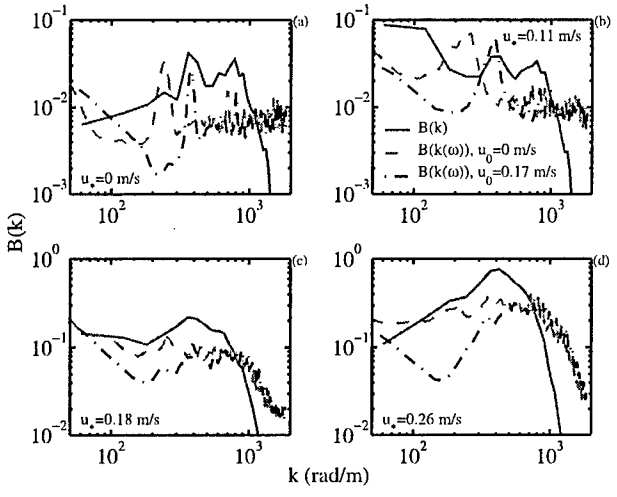

Figure 4. Comparison of measured and converted wave number spectra at different wind speeds. The wind friction velocity is marked in (a)–(d). The effect of orbital advection is designated by u_0; curve designated by $u_0 = 0$ m/s corresponds to the situation in which the orbital advection is ignored.

The main conclusion that the advection of orbital velocity produces a net frequency downshift is not changed.

4. Summary

[13] The ocean surface roughness is contributed mainly by intermediate and short-scale ocean surface waves. The length scale of these waves falls in the region of severe Doppler frequency shift, and the resulting frequency spectrum is subjected to serious distortions, making it difficult to interpret the length scale of a spectral wave component. In this paper, an analysis is presented on the Doppler frequency shift attributable to advection by the orbital velocity of background waves. The effect leads to a net frequency downshift in the encounter frequency spectrum (Figure 3).

[14] Simultaneous spatiotemporal measurements of the surface slope were acquired by a scanning laser slope sensor. Using the data, wave number and frequency spectra can be computed from the same measurements (Figure 1). Considerable differences are found in the two sets of wave number spectra derived from direct spatial measurements and from conversion of the frequency spectrum calculated from the temporal measurements (Figure 4). The result shows that frequency downshifts due to orbital advection may be important in low-wind conditions.

[15] The study of the spectral composition of the ocean surface roughness is of interest to ocean remote sensing and air-sea interaction. Presently, it is recognized that the process of wind-wave generation at low-wind condition requires more research. A better quantification of the ocean surface roughness properties may contribute to the clarification of air-sea interaction processes at low-wind conditions.

[16] **Acknowledgments.** This work is sponsored by the Office of Naval Research (NRL PE61153N and PE62435N). NRL contribution JA-7330-05-5252.

References

Hwang, P. A. (2002), Phase distribution of small scale ocean surface roughness, *J. Phys. Oceanogr.*, *32*, 2977–2987.

Hwang, P. A. (2005), Wave number spectrum and mean square slope of intermediate-scale ocean surface waves, *J. Geophys. Res.*, *110*, C10029, doi:10.1029/2005JC003002.

Hwang, P. A., D. B. Trizna, and J. Wu (1993), Spatial measurements of short wind waves using a scanning slope sensor, *Dyn. Atmos. Oceans*, *20*, 1–23.

Longuet-Higgins, M. S. (1960), Changes in the form of short gravity waves on long waves and tidal currents, *J. Fluid Mech.*, *8*, 565–585.

Phillips, O. M. (1977), *The Dynamics of the Upper Ocean*, 2nd ed., Cambridge Univ. Press, New York.

Phillips, O. M. (1981), The dispersion of short wavelets in the presence of a dominant long wave, *J. Fluid Mech.*, *107*, 465–485.

Phillips, O. M. (1984), On the response of short ocean wave components at a fixed wavenumber to ocean current variations, *J. Phys. Oceanogr.*, *14*, 1425–1433.

Wright, J. W. (1966), Backscattering from capillary waves with application to sea clutter, *IEEE Trans. Antennas Propag.*, *14*, 749–754.

Wright, J. W. (1968), A new model for sea clutter, *IEEE Trans. Antennas Propag.*, *16*, 217–223.

P. A. Hwang, Remote Sensing Division, Naval Research Laboratory, 4555 Overlook Avenue SW, Washington, DC 20375, USA. (phwang@ccs.nrl.navy.mil)